Water Supply

IWA PUBLISHING

Water Supply Vol 22 No 10, 7576 doi: 10.2166/ws.2022.338

Effect of hydraulic conditions on manganese accumulation by physical and chemical pathways in chlorinated water distribution system: A preliminary laboratory study

Xinyi Zhou[a], Tomohiro Nakanishi[a,*], Shinya Echigo[a], Koji Kosaka[b] and Sadahiko Itoh[a]

[a] Department of Environmental Engineering, Graduate School of Engineering, Kyoto University, Kyoto University Katsura, Nishikyo, Kyoto 615-8540, Japan
[b] Department of Environmental Health, National Institute of Public Health, 2-3-6 Minami, Wako, Saitama 351-0197, Japan
*Corresponding author. E-mail: nakanishi.tomohiro.8r@kyoto-u.ac.jp

ABSTRACT

The accumulation of manganese (Mn) in drinking water distribution systems (DWDS) is the main reason for 'black water' occurrences at customers' taps. Here, we focused on the impact of hydraulic conditions on Mn accumulation in well chlorinated DWDS, particularly on the physical pathway (i.e., the attachment of particulate Mn to the inner pipe surface) and the chemical pathway (i.e., the autocatalytic oxidation of Mn^{2+} on the surface of accumulated Mn). Mn accumulation on epoxy resin, a typical lining material for distribution pipes in Japan, was observed in laboratory-scale experiments under different water velocity conditions. The results showed that Mn accumulation was significantly enhanced under higher velocity conditions, which was then fitted with the numerical models describing Mn accumulation by the physical and chemical pathways and the detachment. The rate constants for the physical and chemical pathways had a positive relationship with the flow turbulence in the investigated range, suggesting that hydraulic conditions in DWDS play an important role in Mn accumulation. Effects of Mn speciation and water characteristics on the accumulation process were also simulated under various hydraulic conditions. Based on the obtained results, appropriate countermeasures to control manganese accumulation were then discussed.

Key words: chemical oxidation, drinking water distribution system, hydraulic condition, manganese accumulation, numerical simulation, physical attachment

HIGHLIGHTS

- Effect of hydraulic condition on Mn accumulation in distribution pipes was studied.
- Mn accumulated in pipes via the physical and chemical pathways in chlorinated condition.
- The contribution of the chemical pathway of Mn accumulation increased with time.
- The rates of both pathways were greatly affected by water velocity.
- Increasing the water velocity alone may not be sufficient to reduce Mn accumulation.

GRAPHICAL ABSTRACT

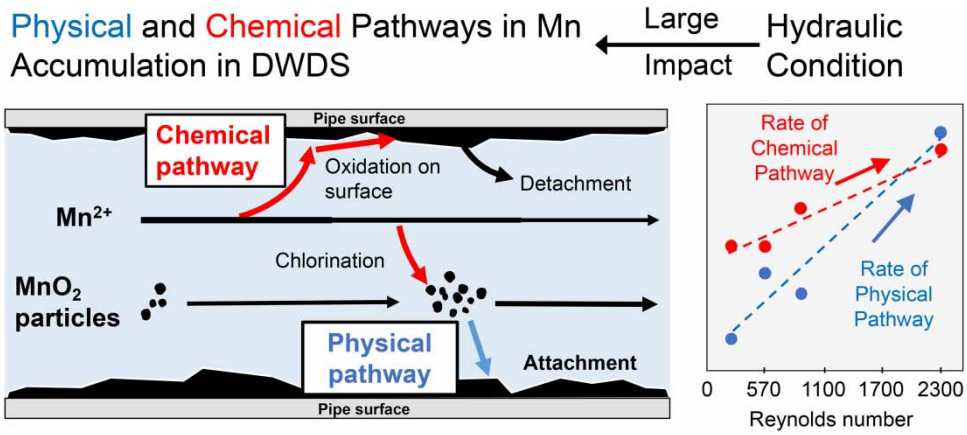

INTRODUCTION

'Black water' is a common discoloration problem of drinking water (Sly *et al.* 1990; Cerrato *et al.* 2006; Li *et al.* 2019), which is caused by the resuspension of accumulated manganese (Mn) on the inner surfaces of drinking water distribution systems (DWDS; Kohl & Medlar 2006). Significant accumulation of Mn has been observed in operational DWDS even when Mn concentration in treated water was as low as approximately 10 $\mu g \cdot L^{-1}$ (Li *et al.* 2019; Ma *et al.* 2019). This is much lower than the typical guideline values of 50 $\mu g \cdot L^{-1}$ or 100 $\mu g \cdot L^{-1}$ worldwide, which complicates controlling Mn accumulation and subsequent discoloration problems.

Mn accumulates in DWDS mainly through the formation of insoluble Mn (i.e., MnO_2) by the reaction between Mn^{2+} ions and residual disinfectants (Sly *et al.* 1990; Kohl & Medlar 2006; Li *et al.* 2019), or through microbial deposition by Mn-oxidizing bacteria (Sly *et al.* 1990; Rygel 2006; Li *et al.* 2022). In well chlorinated DWDS, however, the contribution of biological accumulation is considered to be low because free chlorine effectively inhibits biological processes (Sly *et al.* 1990; Rygel 2006; Ginige *et al.* 2011). We have previously reported that Mn accumulates through two pathways under well chlorinated conditions (Zhou *et al.* 2020): the attachment of particulate Mn (MnO_2) to the inner pipe surface (i.e., the physical pathway) and the autocatalytic oxidation of Mn^{2+} on the surface of accumulated Mn (i.e., the chemical pathway), as shown in Equations (1) and (2) (Hao *et al.* 1991):

$$MnO_2(s) + Mn^{2+} \rightarrow MnO_2 \cdot Mn^{2+}(s) \quad (1)$$

$$MnO_2 \cdot Mn^{2+}(s) + HOCl + H_2O \rightarrow 2\,MnO_2(s) + Cl^- + 3H^+ \quad (2)$$

Because the chemical pathway involves the oxidation of Mn^{2+}, Mn accumulation processes could be affected by water characteristics, e.g., pH and coexistent substances (Hao *et al.* 1991; Allard *et al.* 2013; Li *et al.* 2020), as well as Mn concentration and speciation (Hao *et al.* 1991; Li *et al.* 2019; Zhou *et al.* 2020).

Hydraulic conditions in distribution pipes have been suggested as an important factor in material accumulation in DWDS (Vreeburg & Boxall 2007; van Thienen *et al.* 2011). High water velocity in pipe networks has been claimed to be effective in controlling accumulation of suspended solids by creating high shear stress (Boxall & Saul 2005). Vreeburg (2007) proposed a 'self-cleaning pipe network', in which material accumulation was prevented by achieving the daily maximum water velocity of 0.4 $m \cdot s^{-1}$. Nonetheless, the influence of hydraulic conditions on Mn accumulation has rarely been investigated, except in the study by Sly *et al.* (1988), who examined the effect of water velocity on the development of the Mn-depositing biofilm in DWDS. Furthermore, the effect of hydraulic conditions on the physico-chemical parameters of Mn accumulation, specifically via the aforementioned physical and chemical pathways, has not been studied yet.

The objective of this study was to understand the influence of hydraulic conditions on Mn accumulation through physical, chemical pathways, and Mn detachment. Apart from our previous study (Zhou *et al.* 2020), which tested Mn accumulation in a clean batch system, we set up a semi-continuous system fed with real drinking water to imitate its flowing condition. Kinetics of these processes were then described by a numerical model based on our previous study (Zhou *et al.* 2020), and the effect of hydraulic conditions was formulated. The obtained results underscored the significance of the influence of hydraulic conditions on Mn accumulation in well chlorinated DWDS and helped to suggest appropriate countermeasures for preventing Mn accumulation.

METHODS

Reagents and apparatus

Manganese sulfate ($MnSO_4$), sodium hypochlorite (NaClO), and nitric acid (HNO_3) used in this study were of reagent grade and purchased from FUJIFILM Wako Pure Chemical (Osaka, Japan). A stock solution of $MnSO_4$ (0.5 g-$Mn^{2+} \cdot L^{-1}$) for Mn accumulation experiments was prepared with ultrapure Milli-Q water using a Milli-Q Reference Water Purification System (Merck Millipore; Burlington, MA) and stored at 4 °C in the dark. Pure water (Elix water) used in the detachment experiment was produced by an Elix Advantage Water Purification System (Merck Millipore, Burlington, MA). The tap water used in this study was obtained from a laboratory at Kyoto University.

A laboratory-scale reactor was used to investigate the influence of water hydraulic parameters on Mn accumulation and detachment (Fig. S1 in the Supplementary Materials). It was a vertical acrylic column (length, 70 cm; inner diameter, 2.5 cm), containing a plastic (polyvinyl chloride) holder in the center that held test pieces (1.5 cm in width) on both sides,

which minimized the influence of gravity, a less important contributor to the accumulation of substances in DWDS (Boxall & Saul 2005; Vreeburg 2007). Water was fed from the bottom to the top of the reactor. During the experiments, the reactor was covered to prevent the influence of light. All the experiments were performed at room temperature (20 °C).

Test pieces made of epoxy resin, kindly provided by KUBOTA Corporation (Osaka, Japan), were used in both the accumulation and detachment experiments (see the following sections). This material was selected because it is one of the most common lining materials for ductile iron pipes in Japan (JWWA 2012). Two types of test pieces with different surface areas were used. Eight test pieces with a 7.5 cm^2 (1.5 cm × 5 cm) and 16 test pieces with 22.5 cm^2 (1.5 cm × 15 cm) were evenly inserted on both sides of the plastic holder in the detachment and accumulation experiments, respectively. Vertical difference in Mn accumulation within the reactor was considered negligible because the formed particles were so small that sedimentation would be inhibited by upward water flow. This was partially confirmed during preparation of the detachment experiment (see below).

The reactors and other system components (e.g., tanks and pumps) were soaked in 0.1 M HNO_3 overnight and then rinsed with tap water before use. The test pieces were sonicated for 15 min and then rinsed with Milli-Q water to prevent the introduction of extra particles.

Mn accumulation experiment under various water velocities

One-month accumulation experiments were conducted under various water velocities. Because particulate MnO_2 and Mn^{2+} accumulate through different pathways (Zhou *et al.* 2020), the experimental system had to be set up in such a way so that both these Mn species could exist in the feed water. Considering the water volume required and experimental operation, the experiment was conducted with a semi-continuous (for producing Mn-containing solution) and semi-circulated (for Mn accumulation on test pieces) system (Figure 1). Tap water containing 10 μg·L^{-1} Mn^{2+} and 5 mg·L^{-1} HOCl was continuously pumped into a closed high density polyethylene (HDPE) reaction tank at flow rates of 18 and 2 mL·min^{-1}, respectively. The volume of the solution in the reaction tank was kept at 3.5 L with overflow under mixing conditions to produce Mn solution containing both Mn^{2+} and MnO_2. This Mn solution was then circulated by a pump between the reaction tank and two parallel reactors at constant water velocities, which were adjusted by the valves at the bottom of the reaction tank. The reaction tank, pumps, and connection tubes were regularly exchanged to acid-washed or new ones because Mn was also observed to accumulate on these parts. One test piece was collected twice a week to determine the amount of Mn accumulation over time. Water samples in the reaction tank were collected daily or every other day for water quality analysis, including the concentration and speciation of Mn, pH, and residual Cl_2 in the reaction tank.

The accumulation experiments were performed at four velocities, 0.02, 0.05, 0.08, and 0.20 m·s^{-1}. Reynolds number was estimated from the hydraulic diameter of reactor (as calculated considering the plastic folder inside), kinematic viscosity of water at room temperature (20 °C), and flow velocity. These velocities corresponded to Reynolds numbers ranging from 230 to 2,300, which indicated that the reactors were in laminar to transient flow regimes. Although most of the real

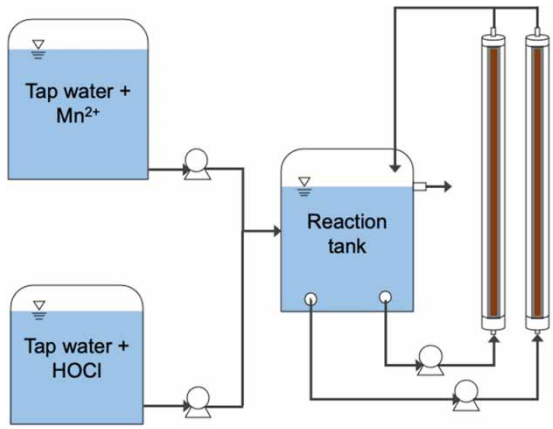

Figure 1 | Schematic diagram of a Mn accumulation experiment.

distribution pipes are considered to be in the turbulent flow regime, we believe that our experimental conditions were still useful for understanding the qualitative effects of flow characteristics on Mn accumulation. The entire study was divided into two groups of experiments. Mn accumulation at water velocities of 0.05 and 0.2 $m \cdot s^{-1}$ was examined in Group 1 experiments, whereas accumulation at velocities 0.02 and 0.08 $m \cdot s^{-1}$ was examined in Group 2 experiments. All experiments lasted for 4 weeks.

Mn detachment experiment under various water velocities

The detachment experiment was conducted in two steps: the formation and detachment of accumulated Mn. The same reactors were used in both steps. Figure S2 shows the schematic of the detachment experiment.

Formation of accumulated Mn (step 1)

Accumulation of Mn that would subsequently detach proceeded under the flowing conditions of tap water containing Mn^{2+} and free chlorine (Fig. S2a). $MnSO_4$ and HOCl were dissolved and mixed in 50 L of tap water in a polyethylene tank with final concentrations of 1 mg-$Mn^{2+} \cdot L^{-1}$ and 6 mg-$Cl_2 \cdot L^{-1}$, respectively. High concentrations of Mn^{2+} and Cl_2 were used to rapidly accumulate Mn on the test pieces. The Mn solution was continuously pumped into four parallel reactors at a water velocity of 0.02 $m \cdot s^{-1}$, and the effluent of the reactors was recirculated to the polyethylene tank (Fig. S2a). To maintain constant water parameters, such as pH, Mn concentration, Mn speciation, and Cl_2 concentration during the accumulation process, the feed water was freshly prepared every day. The entire process lasted for 7 days. Subsequently, test pieces at the top, middle, and bottom of each reactor were collected, and average value of the three positions was calculated to determine the initial amount of Mn in each reactor before detachment. There were no significant differences among the three positions in the amount of accumulated Mn in all reactors.

Detachment of accumulated Mn (step 2)

The plastic holders with test pieces as prepared above were immediately transferred to other clean columns, as shown in Figure S2b. To observe the detachment process selectively, Elix water was used as feed water in this step, as it was expected to contain negligible concentrations of particulate matter and Mn to cause the accumulation process. Elix water (50 L) was pumped into four reactors from a plastic tank at different velocities (0.02, 0.05, 0.15, and 0.30 $m \cdot s^{-1}$). The effluent of the reactors was recirculated into the plastic tank. To prevent the re-attachment of detached Mn from the test pieces, Elix water was exchanged every day in the first week and then every other day. Test pieces were collected in triplicate on days 3, 10, 20, and 30 to observe the time course of the detachment of accumulated Mn.

Analytical methods

Mn that accumulated on the test pieces in all experiments was recovered by soaking each test piece in 90 mL of 1 M HNO_3 for 7 days. The amount of accumulated Mn was calculated from its concentration in the solution. The aqueous Mn in the reaction tank in the accumulation experiments was fractionated into total Mn and soluble Mn. The latter was defined as the fraction less than 0.2 μm in diameter (GL Chromatodisc 13P; GL Science, Tokyo, Japan), whereas the difference between total and soluble Mn (Mn^{2+}) reflected the insoluble Mn (MnO_2). Fractionation was immediately conducted after collecting the water sample to prevent further chlorination of Mn^{2+}. In Group 2, we also investigated Mn samples passed through a 10 kDa membrane (Amicon® Ultra 15 mL Centrifugal Filters – 10 kDa, Merck Millipore) to confirm the solubility of Mn in particles below 0.2 μm in diameter. All the samples for Mn analysis were digested with 0.5 M HNO_3 at 105 °C for 7 h (American Public Health Association (APHA) 2005) and then stored at 4 °C in the dark before analysis. The concentrations of Mn in the samples were measured by inductively coupled plasma mass spectrometry (Xseries 2Xt, Thermo Fisher Scientific; Waltham, MA). The pH was measured using a pH meter (pH METER D-51, Horiba, Kyoto, Japan). Residual chlorine was analyzed by the *N*,*N*-diethyl-*p*-phenylenediamine colorimetric method using a residual Cl_2 meter (AQ-201, SIBATA; Saitama, Japan).

Statistical analysis

Differences between the initial and residual amounts of accumulated Mn in the detachment experiment and between the concentrations of Mn in particles below 0.2 μm in diameter and in solutions passed through the 10 kDa membrane in Group 2 of the Mn accumulation experiments were analyzed using the paired Student's *t*-test. The parametric one-way analysis of

variance and Bonferroni *P*-value corrected *t*-test were performed using Python package statsmodels (https://www.statsmodels.org/) (Seabold & Perktold 2010) to test the difference between fractions of detached Mn after 30-day detachment experiments under each examined water velocity. Differences were considered statistically significant when $P < 0.05$.

Numerical modeling of the Mn accumulation process

The obtained experimental results were incorporated into a numerical model established in our previous study that described the accumulation of Mn via the physical and chemical pathways (Zhou *et al.* 2020). Equation (3) shows the general equation for the Mn accumulation process in the present model. The first two terms represent the rates of Mn accumulation via the physical and chemical pathways, respectively. The third term represents the detachment rate:

$$\frac{\mathrm{dMn_{sur}}}{\mathrm{d}t} = \frac{\mathrm{dMn_p}}{\mathrm{d}t} + \frac{\mathrm{dMn_c}}{\mathrm{d}t} - \frac{\mathrm{dMn_d}}{\mathrm{d}t} \tag{3}$$

where $\mathrm{Mn_{sur}}$ ($\mathrm{mol{\cdot}cm^{-2}}$), $\mathrm{Mn_p}$ ($\mathrm{mol{\cdot}cm^{-2}}$), $\mathrm{Mn_c}$ ($\mathrm{mol{\cdot}cm^{-2}}$), and $\mathrm{Mn_d}$ ($\mathrm{mol{\cdot}cm^{-2}}$) are the amount of total accumulated Mn on a unit surface area, amount accumulated via the physical pathway, amount accumulated via the chemical pathway, and amount of detached Mn, respectively. Equation (4) represents the rate of Mn accumulation via the physical pathway:

$$\frac{\mathrm{dMn_p}}{\mathrm{dt}} = \left(K_{\mathrm{att}} \cdot [\mathrm{MnO_2}] \cdot \frac{A}{v}\right) \cdot \frac{v}{A} \tag{4}$$

where K_{att} ($\mathrm{cm^{-2}Ls^{-1}}$) is the rate constant of the physical pathway; $[\mathrm{MnO_2}]$ (M) is the concentration of $\mathrm{MnO_2}$ in the solution passing through the reactor; A ($\mathrm{cm^2}$) is the surface area of the test pieces; v (L) is the volume of the reactor. The term in brackets represents the decrease in $\mathrm{MnO_2}$ in the solution. The rate of Mn accumulation in the chemical pathway is shown in Equation (5):

$$\frac{\mathrm{dMn_c}}{\mathrm{d}t} = k_{\mathrm{sur}} \cdot [\mathrm{OH^-}] \cdot [\mathrm{HOCl}] \cdot \alpha_{\mathrm{Cl}} \cdot [\mathrm{Mn^{2+}}] \cdot \mathrm{Mn_{sur}} \tag{5}$$

where k_{sur} ($\mathrm{M^{-3}s^{-1}}$) is the rate constant for autocatalytic oxidation on the surface (i.e., the chemical pathway); $[\mathrm{Mn^{2+}}]$ (M) is the concentration of $\mathrm{Mn^{2+}}$ in the solution passing through the reactor; $[\mathrm{OH^-}]$ (M) is the concentration of $\mathrm{OH^-}$ calculated from pH; [HOCl] (M) is the total $\mathrm{Cl_2}$ concentration; and α_{Cl} is the fraction of HOCl to total $\mathrm{Cl_2}$ based on pH, as shown in Equation (6):

$$\alpha_{\mathrm{Cl}} = \frac{1}{10^{(\mathrm{pH} - pKa)} + 1} \tag{6}$$

where $\mathrm{p}K\mathrm{a} = 7.53$ (Hao *et al.* 1991).

Zhou *et al.* (2020) observed that the rate constants of autocatalytic oxidation (k_{sur}) were negatively related to the total Mn concentration in bulk water, which may be because of the difference in the specific surface area of $\mathrm{MnO_2}$ particles. Therefore, the relationship between k_{sur} and the total Mn concentration was empirically obtained through preliminary studies (Supplementary Text S1), in which Mn accumulation under different total Mn concentrations was investigated in batch experiments similar to those in our previous studies (Zhou *et al.* 2020). The fitting results showed that k_{sur} was a negative power function of the total Mn concentration with a power index of -1.7. Thus, Equation (7) represents k_{sur}, in which c ($\mathrm{M^{-1.3}\,s^{-1}}$) is the coefficient of k_{sur} in the reactor:

$$k_{\mathrm{sur}} = c \cdot ([\mathrm{MnO_2}] + [\mathrm{Mn^{2+}}])^{-1.7} \tag{7}$$

The rate of the detachment of accumulated Mn was assumed to be a first-order reaction, as shown in Equation (8):

$$\frac{\mathrm{dMn_d}}{\mathrm{d}t} = K_{\mathrm{det}} \cdot \mathrm{Mn_{sur}} \tag{8}$$

where K_{det} (s^{-1}) is the rate constant of the detachment. Through model fitting, we assumed that water characteristics such as [Mn^{2+}], [MnO_2], [HOCl], and pH in the reactor were homogenous, and their changes along the reactor were considered negligible compared to those in the reaction tank during operation. The changes in water characteristics in the reaction tank were assumed to be linear in relation to time between the two analyses, as shown in Equation (9):

$$\frac{dWQ}{dt} = \frac{WQ_{t2} - WQ_{t1}}{\Delta T} \quad (9)$$

where WQ refers to [Mn^{2+}], [MnO_2], [HOCl], or pH in each case; ΔT (s) is the time interval between the two analyses of water quality (i.e., t_1 and t_2). The initial tap water characteristics were set at the following values: 0 $\mu g \cdot L^{-1}$ for [Mn^{2+}] and [MnO_2], 0.1 mg-$Cl_2 \cdot L^{-1}$ for [HOCl], and 7.6 for pH.

The values of K_{det}, K_{att}, and c were independently estimated for each water velocity by fitting the equations to the experimental results. First, K_{det} was estimated by fitting the integrated form of Equation (8) to the results of the detachment experiment, and the relationship between K_{det} and water velocity was formulated. Incorporating this relationship into Equations (3)–(8), the values of K_{att} and c were estimated based on the accumulation experiment results. The week 1 results of the accumulation experiments were used for estimating the K_{att} value, because the initial contribution of the chemical pathway was considered negligible (Zhou *et al.* 2020). Finally, the value of c was obtained by fitting the entire set of the accumulation experiment results. The details of the fitting procedures are shown in Supplementary Text S2.

RESULTS

Mn detachment under different water velocities

Figure 2 shows the relative decrease in the residual amount of Mn normalized by the initially accumulated amount in the detachment experiments (see Fig. S5 for the raw data before normalization). The initial amount of accumulated Mn on the test pieces was 12 ± 2.4 $\mu g \cdot cm^{-2}$. After 30 days of operation, 50, 61, 78, and 91% of the initially accumulated amount of Mn was detached under water velocities of 0.02, 0.05, 0.15, and 0.30 $m \cdot s^{-1}$, respectively. These detached Mn fractions were significantly different (Bonferroni-adjusted $P < 0.05$), indicating that high water velocity enhanced the detachment process.

The above results were successfully fitted with the integrated form of Equation (8) with R^2 values larger than 0.9 being obtained under all examined water velocities (Supplementary Text S2; Fig. S6). Moreover, the relationship between K_{det}

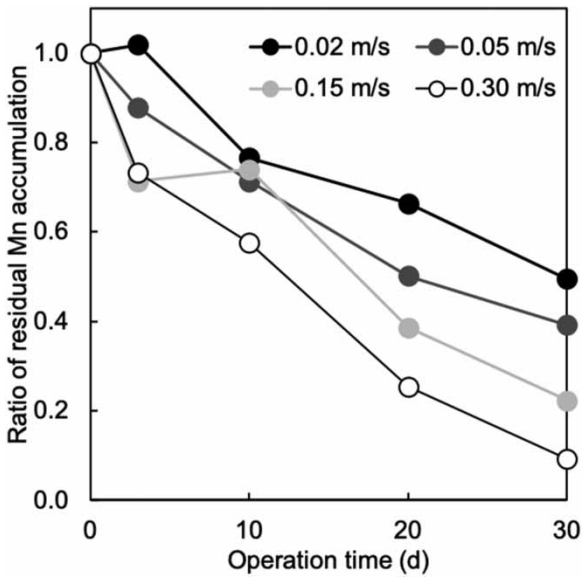

Figure 2 | Decrease in the residual amount of accumulated Mn under each velocity condition in detachment experiments. Data are presented as average values ($n = 3$).

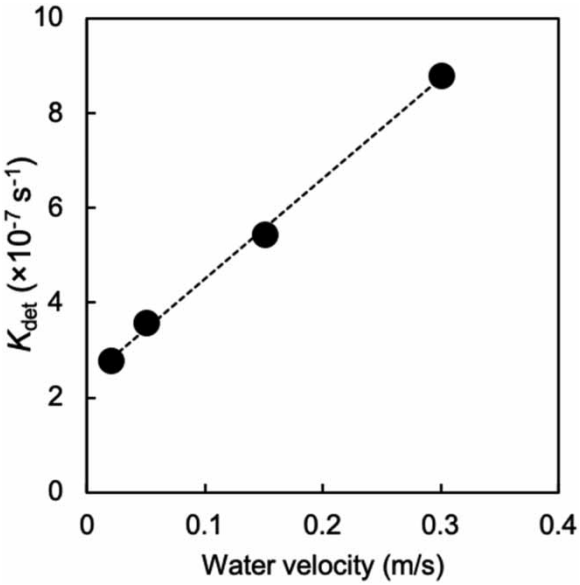

Figure 3 | Linear relationship between the rate constant of the detachment (K_{det}) and tested water velocity.

and water velocity was found to be linear in the tested velocity range (Figure 3). Therefore, the relationship could be formulated as follows:

$$K_{det} = 2.1 \times 10^{-6} \cdot U + 2.4 \times 10^{-7} \quad (10)$$

where U (m·s^{-1}) is water velocity in the reactor.

Results of Mn accumulation experiments under different water velocities

The water characteristics in the reaction tank were monitored daily or every other day. pH was stable in both groups, being 7.5 ± 0.12 (error: standard deviation; the same below) in Group 1 and 7.7 ± 0.24 in Group 2. Residual Cl_2 became stable at 0.62 ± 0.15 mg-Cl_2·L^{-1} and 0.9 ± 0.3 mg-Cl_2·L^{-1} (before day 22) in Groups 1 and 2, respectively (Fig. S7). In contrast, because of Mn accumulation in the whole system (i.e., reactor walls, tubing, and pumps), the total Mn concentration in the reaction tank decreased in the first week from 6.0 and 10 μg·L^{-1} to 0.73 and 1.6 μg·L^{-1} in Groups 1 and 2, respectively, and then stabilized at these low concentrations (Fig. S8). The sudden increase in the concentrations of total Mn and residual Cl_2 in Group 2 was due to the temporal stoppage of pumps for system maintenance. The concentration of Mn particles below 0.2 μm in diameter also decreased in the first week and then stabilized at 0.57 ± 0.16 and 0.80 ± 0.66 μg·L^{-1} in Groups 1 and 2, respectively (Fig. S8). Mn concentrations in the fraction that passed through 0.2 μm pore size and those that passed through 10 kDa membrane in Group 2 were not significantly different ($P > 0.05$, Fig. S9), suggesting that most Mn smaller than 0.2 μm pore size were also smaller than 10 kDa. As it is technically difficult to discriminate ionic and colloidal Mn in such a small size range, the fraction of Mn smaller than 0.2 μm pore size was considered as Mn^{2+} in this study.

Figure 4 shows the observed time courses of Mn accumulation under different water velocities. Within week 1, Mn accumulated linearly with time in all the velocity conditions. Mn accumulation then tended to accelerate over time, especially when the velocity was set at 0.2 m·s^{-1}. The final accumulated amounts after a total of 28 days in operation were 0.44, 0.82, 0.97, and 2.8 μg·cm^{-2} for the water velocities of 0.02, 0.05, 0.08, and 0.2 m·s^{-1}, respectively. Importantly, higher water velocity (especially at 0.2 m·s^{-1}) led to a larger amount of accumulation throughout the experiment.

Model fitting to the results of accumulation experiments

Using the relationship between K_{det} and water velocity (Equation 10), independent pairs of K_{att} and c values were estimated for each water velocity condition by model fitting, as shown in Figure 5. The estimated values of K_{att} and c are summarized in Table S3. K_{att} and c could be linearly formulated to the water velocity and Reynolds number (Figure 6), as shown in Equations

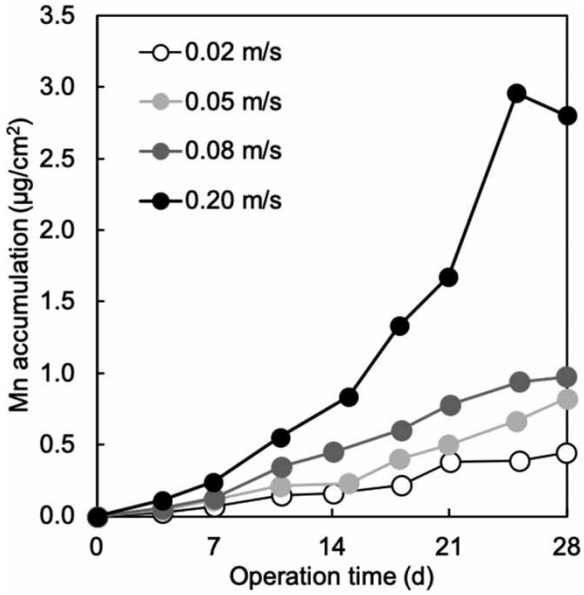

Figure 4 | Increase in Mn accumulation under different water velocity conditions ($n = 1$).

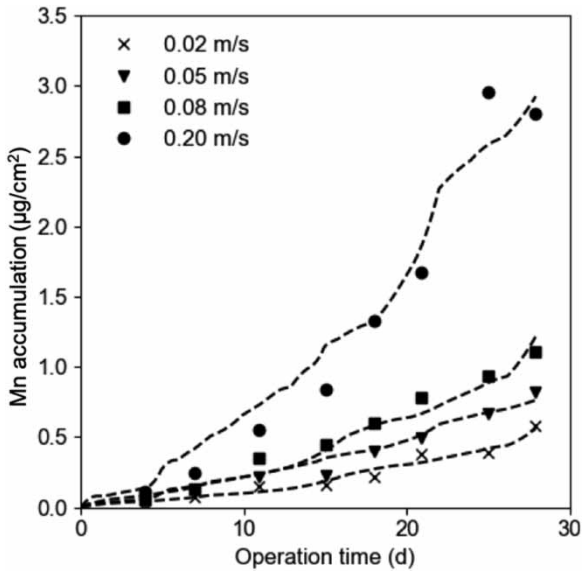

Figure 5 | Predicted Mn accumulation at different water velocities.

(11) and (12), respectively.

$$K_{att} = 2.8 \times 10^{-6} \cdot U + 4.2 \times 10^{-8} \tag{11}$$

$$c = 2.6 \times 10^{1} \cdot U + 4.9 \tag{12}$$

In the range of the examined flow conditions, the c value ranged from 5.6 to 10 $M^{-1.3} s^{-1}$, which was one order of magnitude smaller than that that obtained in preliminary experiments using conical flasks, 1.0×10^{2} $M^{-1.3}$ s^{-1} (Table S2). In contrast, K_{att} ranged from 9.1×10^{-8} to 6.2×10^{-7} cm^{-2} Ls^{-1}, which was larger than that in preliminary experiments,

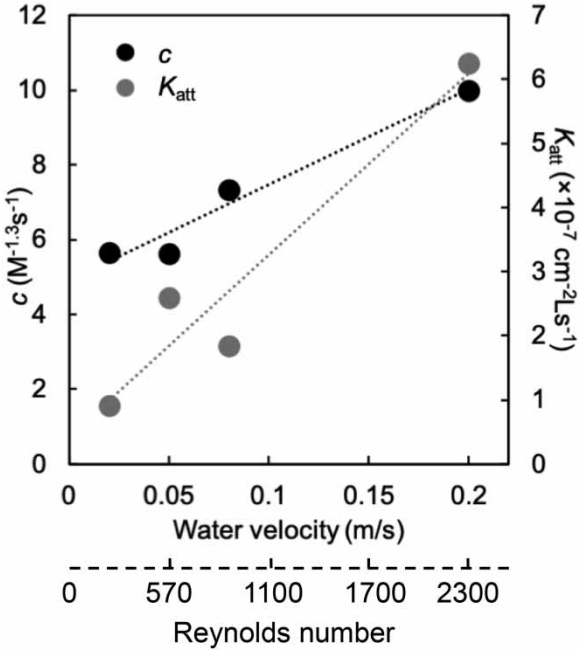

Figure 6 | Effect of water velocity and Reynolds number on the chemical pathway (c) and the physical pathway (K_{att}).

1.6×10^{-8} cm^{-2} Ls^{-1} (Table S2). The comparison suggested that different experimental conditions significantly impacted the two separate pathways of accumulation.

DISCUSSION

Presence of physical and chemical pathways of Mn accumulation

In this study, the effects of hydraulic conditions on the physical and chemical pathways of Mn accumulation were investigated for the first time. In the accumulation experiments, the characteristics of water flowing into the reactors were controlled so that both Mn^{2+} and MnO_2 were present. Consequently, Mn accumulation increased linearly with time approximately during the first 7 days of operation, and after that time point, it accelerated, especially at the water velocity of 0.2 $m{\cdot}s^{-1}$ (Figure 4). Although such acceleration is often explained by the biological accumulation through Mn-oxidizing bacteria (Sly *et al.* 1990; Li *et al.* 2022), biological processes most likely were negligible in our experiments because the residual chlorine was maintained at a high concentration ($0.6 - 0.8$ $mg{\cdot}L^{-1}$) (Fig. S7). Therefore, these observations strongly indicate the presence of two pathways of Mn accumulation: the physical pathway, in which MnO_2 particles attached to the surface linearly with respect to time, and the chemical pathway, i.e., the autocatalytic oxidation of Mn^{2+} on the surface of accumulated Mn (Equations (1) and (2)). The presence of these two pathways was also observed in our previous study (Zhou *et al.* 2020).

As mentioned in the Results section, the estimated values for K_{att} and c in the accumulation experiments using reactors (Table S3) were 5.7–39 times larger and 10–18 times smaller than those obtained in preliminary experiments using conical flasks (Table S2), respectively. The dissimilarity of K_{att} values can be attributed to the differences in the surface-to-volume ratios, which are higher in the reactor than in the conical flasks. The higher surface-to-volume ratio of the reactor might have led to enhanced transportation of MnO_2 particles via the physical pathway.

In contrast, the lower rates of the chemical pathway in the reactors were presumably caused by the differences in water matrix: tap water and carbonate buffer (0.5 mM $NaHCO_3$) were used in the reactor and conical flasks, respectively. The hardness of tap water was approximately 40 $mg{\cdot}L^{-1}$ (Kyoto Water Supply and Sewage Bureau 2020), which suggests the presence of Ca^{2+} and Mg^{2+} cations. Huangfu *et al.* (2013) reported that even low concentrations of Ca^{2+} and Mg^{2+} (i.e., <1 mM) were significantly more efficient than 10 mM Na^+ in enhancing the aggregation of MnO_2 particles. Thus, larger MnO_2 particles might have formed in the tap water than in the carbonate buffer in the preliminary experiments (Text S1), which could lead to the deceleration of autocatalytic oxidation because of the lower specific surface area of the formed MnO_2.

Effect of flow regimes on the Mn accumulation process

The flow in the accumulation experiments was mostly laminar, except in the fastest, 0.2 $m \cdot s^{-1}$ condition, which could be considered as transient to turbulent flow. Although operational DWDSs are generally considered to be within the turbulent flow regime, we selected these low velocity conditions as it was difficult to control the speciation of Mn (the proportion of Mn^{2+} to total Mn) in the feed water under high turbulence in the current experimental setup. Thus, our results below are limited to non-turbulent conditions. However, such conditions are still possible in the distal areas that have lower water velocities and hence relevant.

According to the experimental results, the higher water velocity promoted both the detachment (Figure 2, Fig. S5) and the total accumulated Mn (Figure 4). The rate constants and related coefficients (c, K_{att}, and K_{det}) also positively correlated with water velocity and Reynolds number in the examined ranges (Equations (10)–(12), Figures 3 and 6). These observations indicate that flow conditions strongly influenced the physical and chemical pathways of Mn accumulation and detachment of the accumulated Mn.

Detachment is likely to be caused by the sheer force near the surface of the pipes, which is formed by the velocity gradient perpendicular to the surface, and it becomes more pronounced with an increased water flow velocity in the pipe. Thus, the higher water velocity in the detachment experiments enhanced the detachment process. However, despite this relationship, the total amount of accumulated Mn was still higher under the higher water velocity conditions, which means that the enhancement of the physical and chemical pathways of Mn accumulation was more dominant than that of the detachment process.

As for the physical pathway (i.e., the attachment of MnO_2 to the surface), a particularly high K_{att} value was estimated at the water velocity of 0.2 $m \cdot s^{-1}$ compared to those at the lower velocities (0.02, 0.05, and 0.08 $m \cdot s^{-1}$) conditions (Figure 6). Considering that the flow regime at 0.2 $m \cdot s^{-1}$ condition was transient flow, turbulent diffusion of MnO_2 particles to the surface of the test pieces was likely to be more significant than at lower velocities and laminar flow conditions. A similar trend was also reported for initial bacterial adhesion to plastic materials (Saur *et al.* 2017).

The chemical pathway (i.e., autocatalytic oxidation of Mn^{2+} on the pipe surface) is considered to involve two steps: the adsorption of Mn^{2+} to accumulated MnO_2 (i.e., the formation of $MnO_2 \cdot Mn^{2+}$) and subsequent oxidation of $MnO_2 \cdot Mn^{2+}$ (Equations (1) and (2)). The rates of both processes are extremely rapid (Hao *et al.* 1991; Van Benschoten 1993), which means that the transport of Mn^{2+} and HOCl to the surface of accumulated MnO_2 is the rate-limiting step in the chemical pathway. Therefore, as in the physical pathway, the enhanced transport of chemical species triggered by higher turbulence might be the main reason for the positive impact of water velocity on the chemical pathway.

Contributions of the physical and chemical pathways and detachment

Using the estimated values of c, K_{att}, and K_{det} at each velocity condition, the numerical model quantitatively predicted the contributions of each Mn turnover process to Mn accumulation. Figure 7 shows the predicted results for different water velocities in the accumulation experiments. Consistent with our previous study (Zhou *et al.* 2020), the physical pathway was the only contributor during the initial phase of Mn accumulation for all experimental conditions, followed by the contribution of the increasingly important chemical pathway. With this increasing importance, the chemical pathway became the main contributor to Mn accumulation from the middle to the end of the operation time. Moreover, the detachment process also accelerated with an increased amount of accumulated Mn and became very important in regulating the Mn accumulation process over time.

The predictions show that Mn accumulation via the chemical pathway continued to accelerate during the 1-month accumulation experiments. However, during the longer-term operation, it can be expected that the surface of accumulated MnO_2 available for Mn^{2+} adsorption would not increase anymore after MnO_2 completely covered the surface of the test pieces. Therefore, this acceleration would be limited by the increasing amount of accumulated Mn (Hao *et al.* 1991; Zhou *et al.* 2020), and the entire Mn accumulation process would reach a steady state during the longer-term operation.

Long-term prediction of Mn accumulation in the experimental conditions

We simulated the long-term Mn accumulation process (up to 1 year) under the experimental conditions for further discussion. As described in the previous section, the chemical pathway would no longer accelerate after the significant increase in accumulated Mn on the surface. Therefore, as shown in Equations (13) and (14), we introduced a threshold of accumulated amount (ac, $\mu g \cdot cm^{-2}$), above which the rate of the chemical pathway would be only proportional to Mn^{2+} concentration.

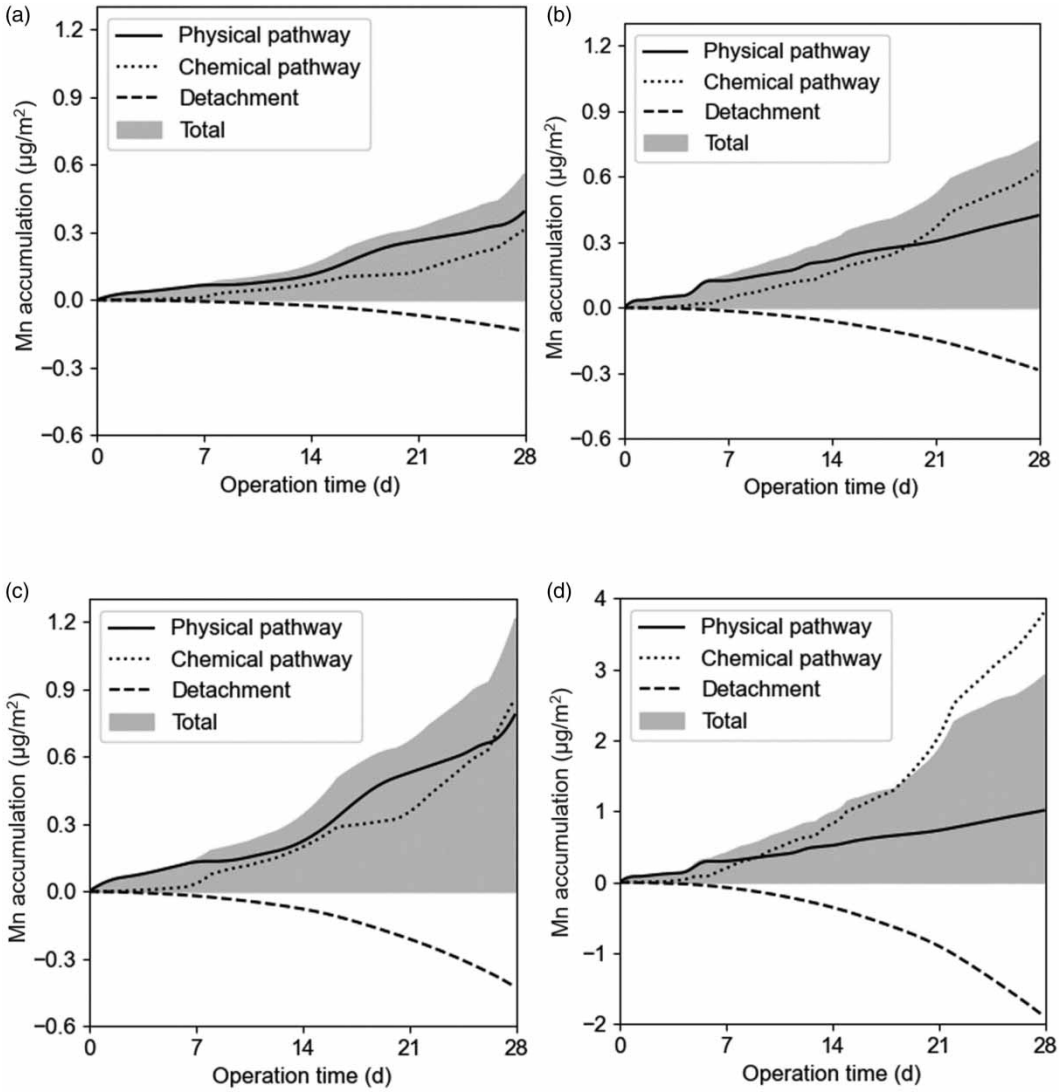

Figure 7 | Predicted contribution of each Mn behavior to the total amount of accumulated Mn at water velocities of (a) 0.02, (b) 0.05, (c) 0.08, and (d) 0.2 m·s^{-1}.

The threshold was set as 5 μg·cm^{-2}, because over this amount, the entire test piece surface was observed to be covered by brown MnO_2:

$$\frac{d\mathrm{Mn_c}}{dt} = k_{\mathrm{sur}} \cdot [\mathrm{OH^-}] \cdot [\mathrm{HOCl}] \cdot \alpha_{\mathrm{Cl}} \cdot [\mathrm{Mn^{2+}}] \cdot \mathbf{Mn'_{sur}} \tag{13}$$

$$\mathbf{Mn'_{sur}} = \begin{cases} \mathrm{Mn_{sur}} & \mathrm{Mn_{sur}} < ac \\ ac & \mathrm{Mn_{sur}} \geq ac \end{cases} \tag{14}$$

Figure 8 shows the 1-year prediction of accumulation in a reactor with two cases of Mn speciation, assuming no temporal fluctuations of water characteristics. When the proportion of Mn^{2+} to the total Mn was 90% (Figure 8(b)), the amount of accumulation at the steady state was approximately 3–10 times larger than when that proportion comprised 10% (Figure 8(a)). This is because accumulation via the chemical pathway became dominant due to the abundance of Mn^{2+}, suggesting the importance of Mn species in water for the accumulation process (Zhou *et al.* 2020).

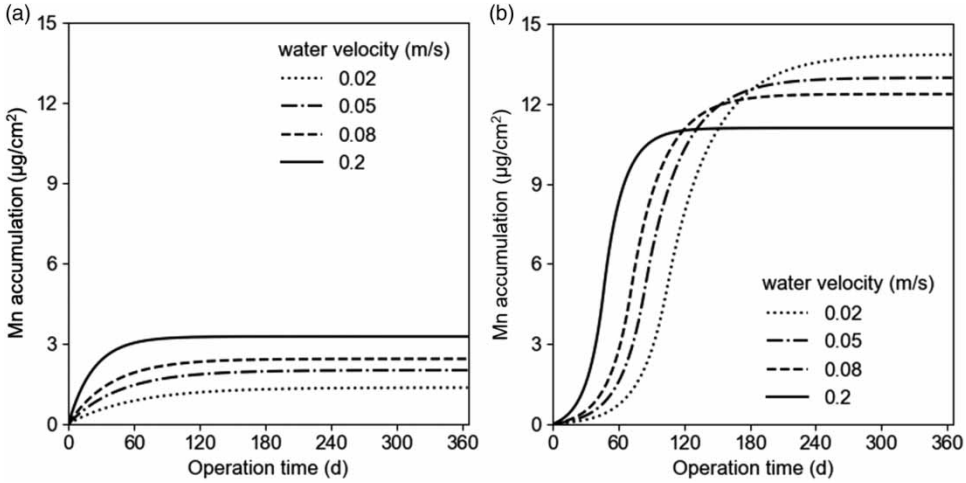

Figure 8 | Predicted amounts of Mn accumulated in the reactor over a 1-year period at different water velocities when the fraction of Mn^{2+} out of total Mn amount comprises (a) 10% and (b) 90%. Prediction conditions: pH = 7.6; HOCl = 0.7 mg·L^{-1}; total Mn = 3 μg·L^{-1}.

Furthermore, during the initial period of accumulation (until approximately day 100), the large water velocity enhanced the accumulation process regardless of Mn speciation because the higher water velocity promoted accumulation via both the physical and chemical pathways, whereas the initial contribution of detachment was lower (Figure 7). On the other hand, the effect of water velocity at a steady state was opposite between two cases of Mn speciation (Figure 8): positive or negative effects were observed under the lower and higher Mn^{2+} concentrations, respectively. This is due to the differences in slopes of the linear relationships between water velocity and the rates of physical and chemical pathways (Figure 6), in which the impact of velocity was larger on K_{att} than on the c value. When Mn^{2+} proportion was low (Figure 8(a)), the positive impact of velocity on the physical pathway was stronger than on the detachment. On the other hand, in the case of high proportions of Mn^{2+} (Figure 8(b)), the positive impact of velocity on the chemical pathway was lower than on the detachment, leading to the tendency opposite to that seen in the case of low relative Mn^{2+} level. Further predictions at steady state (Fig. S10) showed that the effect of water velocity was dependent on water characteristics (i.e., pH, HOCl concentration, and Mn speciation). In general, the positive influence of water velocity was expected when the water characteristics were less suitable for the chemical pathway to take place, i.e., lower pH, HOCl concentration, and Mn^{2+} proportion. To summarize, these predictions showed that high water velocity could enhance the Mn accumulation process, especially at the initial phase, whereas the subsequent effect of high water velocity would vary depending on the related water parameters.

Practical implications

All the above laboratory-scale results, particularly those that higher water velocity caused larger accumulation, should be interpreted with caution to discuss Mn accumulation in full-scale DWDS. The net effect of water velocity on Mn accumulation in actual pipes would depend on the balance of two positive impacts of water velocity, i.e., those on each accumulation pathway and those on the detachment. Therefore, further research is needed to estimate these effects in actual operational DWDS quantitatively. Nonetheless, it is still very likely that the water flow regime in DWDS can greatly affect the physical and chemical pathways of Mn accumulation. These possibilities are consistent with the previous field observation by Ma *et al.* (2019), in which they analyzed the deposits in distribution pipes at various distances from a water treatment plant. They observed that Mn accumulation was significantly higher at the sites closer to the plant and lower at the sites further away from the plant, which differed from the profiles observed for other elements (Al, Si, and Fe). Although the authors speculated that the higher residual chlorine and soluble Mn concentration in upstream pipes contributed to the faster chemical oxidation and deposition of Mn, the enhancement of the physical and chemical pathways by higher water velocities in upstream pipes can also be considered as a reason, considering that water velocity is generally higher in the upstream pipes (as also shown by the authors). This preferential accumulation of Mn in the upstream pipes was also reported by Li *et al.* (2018). Therefore, our results suggest that just increasing the daily water velocity in DWDS

may not be a very effective countermeasure for controlling the Mn accumulation, although it is a common strategy for reducing the suspended solids deposition (Vreeburg 2007). Our predictions also indicated that the less suitable water characteristics for the chemical pathway would lead to a lower amount of accumulated Mn (Figure 8, Fig. S10). Thus, adjusting the Mn speciation and water parameters in the treated water could be another option to control Mn accumulation.

We investigated the effect of water hydraulic conditions on Mn accumulation, assuming an ideal situation. It should be noted, however, that several important aspects of actual DWDS were not considered. First, the effect of water velocity and related phenomena might be quite different in case of the low residual chlorine concentration because microorganism-mediated accumulation would become dominant (Li *et al.* 2022). It also has been suggested that the detachment of accumulated matters is affected by daily fluctuations of hydraulic conditions (Boxall & Saul 2005), which was also not considered in this study. These aspects should be investigated in future research to achieve better understanding of the effect of water hydraulics on Mn accumulation.

CONCLUSIONS

In this study, we investigated the influence of water hydraulic conditions on Mn accumulation process in well chlorinated distribution systems. The major findings are summarized as follows:

- Experiments and modeling analysis confirmed the existence of the physical and chemical pathways for Mn accumulation. In particular, the contribution of the chemical pathway was found to increase with time, leading to accelerated accumulation.
- The rates of the physical and chemical pathways and that of detachment positively correlated with water velocity in the current experimental setup, suggesting that the hydraulic conditions of the DWDS would play an important role in Mn accumulation and detachment.
- Long-term prediction of the accumulation experiments indicated that large water velocities promote Mn accumulation, especially in the early stages, but that subsequent effects were variable, depending on the associated water characteristics. It was noted that maintaining high water velocities in DWDS, the common countermeasure against the suspended solids accumulation, might not be appropriate for controlling Mn accumulation.
- It was also predicted that adjusting the Mn speciation in the treated water, i.e., reducing the proportion of Mn^{2+} to total Mn, would effectively control the Mn accumulation in DWDS, as also suggested in our previous study (Zhou *et al.* 2020).

ACKNOWLEDGEMENTS

This work was partially supported by grant 18H05918 from the Japan Society for the Promotion of Science (JSPS) KAKENHI. The authors would like to thank KUBOTA Corporation for kindly providing the test pieces of the pipe materials.

DATA AVAILABILITY STATEMENT

All relevant data are included in the paper or its Supplementary Information.

CONFLICT OF INTEREST

The authors declare there is no conflict.

REFERENCES

Allard, S., Fouche, L., Dick, J., Heitz, A. & von Gunten, U. 2013 Oxidation of manganese(II) during chlorination: role of bromide. *Environ. Sci. Technol.* **47** (15), 8716–8723. https://doi.org/10.1021/es401304r.

APHA/AWWA/WEF 2005 *Standard Methods for the Examination of Water and Wastewater*, 21st edn. American Public Health Association/American Water Works Association/Water Environment Federation, Washington DC, USA.

Boxall, J. B. & Saul, A. J. 2005 Modeling discoloration in potable water distribution systems. *J. Environ. Eng.* **131** (5), 716–725. https://doi.org/10.1061/(ASCE)0733-9372(2005)131:5(716).

Cerrato, J. M., Reyes, L. P., Alvarado, C. N. & Dietrich, A. M. 2006 Effect of PVC and iron materials on Mn(II) deposition in drinking water distribution systems. *Water Res.* **40** (14), 2720–2726. https://doi.org/10.1016/j.watres.2006.04.035.

Ginige, M. P., Wylie, J. & Plumb, J. 2011 Influence of biofilms on iron and manganese deposition in drinking water distribution systems. *Biofouling* **27** (2), 151–163. https://doi.org/10.1080/08927014.2010.547576.

Guidelines for Designing Water Supply Facilities 2012 Japan Water Works Association, Tokyo, Japan (in Japanese).

Hao, O. J., Davis, A. P. & Chang, P. H. 1991 Kinetics of manganese (II) oxidation with chlorine. *J. Environ. Eng.* **117** (3), 359–374. https://doi.org/10.1061/(ASCE)0733-9372(1991)117:3(359).

Huangfu, X., Jiang, J., Ma, J., Liu, Y. & Yang, J. 2013 Aggregation kinetics of manganese dioxide colloids in aqueous solution: influence of humic substances and biomacromolecules. *Environ. Sci. Technol.* **47** (18), 10285–10292. https://doi.org/10.1021/es4003247.

Kohl, P. M. & Medlar, S. J. 2006 *Occurrence of Manganese in Drinking Water and Manganese Control*. AWWA Research Foundation, Denver, USA.

Kyoto Water Supply and Sewage Bureau 2022 *Results of Weekly Testing of tap Water Quality*. Available from: https://www.city.kyoto.lg.jp/suido/page/0000159014.html (in Japanese) (accessed May 20, 2022).

Li, G., Ding, Y., Xu, H., Jin, J. & Shi, B. 2018 Characterization and release profile of (Mn, Al)-bearing deposits in drinking water distribution systems. *Chemosphere* **197**, 73–80. https://doi.org/10.1016/j.chemosphere.2018.01.027.

Li, G., Ma, X., Chen, R., Yu, Y., Tao, H. & Shi, B. 2019 Field studies of manganese deposition and release in drinking water distribution systems: insight into deposit control. *Water Res.* **163** (15), 114897. https://doi.org/10.1016/j.watres.2019.114897.

Li, G., Pan, W., Zhang, L., Wang, Z., Shi, B. & Giammar, D. E. 2020 Effect of Cu(II) on Mn(II) oxidation by free chlorine to form Mn oxides at drinking water conditions. *Environ. Sci. Technol.* **54** (3), 1963–1972. https://doi.org/10.1021/acs.est.9b06497.

Li, G., Su, Y., Wu, B., Han, G., Yu, J., Yang, M. & Shi, B. 2022 Initial formation and accumulation of manganese deposits in drinking water pipes: investigating the role of microbial-mediated processes. *Environ. Sci. Technol.* **56** (9), 5497–5507. https://doi.org/10.1021/acs.est.1c08293.

Ma, X., Li, G., Yu, Y., Chen, R., Zhang, Y., Tao, H., Zhang, G. & Shi, B. 2019 Spatial variation of loose deposit characteristics in a 40km long operational drinking water distribution system. *Environ. Sci.: Water Res. Technol.* **5**, 1689–1698. https://doi.org/10.1039/C9EW00391F.

Rygel, A. C. 2006 *Manganese in Drinking Water Distribution Systems*. *PhD thesis*, Dalhousie University, Halifax, Canada.

Saur, T., Morin, E., Habouzit, F., Bernet, N. & Escudié, R. 2017 Impact of wall shear stress on initial bacterial adhesion in rotating annular reactor. *PLOS ONE* **12** (2), e0172113. https://doi.org/10.1371/journal.pone.0172113.

Seabold, S. & Perktold, J. 2010 Statsmodels: Econometric and statistical modeling with python. In: *Proceedings of the 9th Python in Science Conference (SCIPY 2010)*.

Sly, L. I., Hodgkindon, M. C. & Arunpairojana, V. 1988 Effect of water velocity on the early development of manganese-depositing biofilm in a drinking-water distribution system. *FEMS Microbiol. Ecol.* **4** (3–4), 175–186. https://doi.org/10.1111/j.1574-6968.1988.tb02662.x.

Sly, L. I., Hodgkinson, M. C. & Arunpairojana, V. 1990 Deposition of manganese in a drinking water distribution system. *Appl. Environ. Microbiol.* **56** (3), 628–639. https://doi.org/10.1128/AEM.56.3.628-639.1990.

Van Benschoten, J. E. 1993 Discussion of 'kinetics of manganese(II) oxidation with chlorine' by Oliver J. Hao, Allen P. Davis, and Peter H. Chang (May/June 1991, Vol. 117, No. 3). *J. Environ. Eng.* **119** (2), 392–395. https://doi.org/10.1061/(ASCE)0733-9372(1993)119:2(392).

van Thienen, P., Vreeburg, J. H. G. & Blokker, E. J. M. 2011 Radial transport processes as a precursor to particle deposition in drinking water distribution systems. *Water Res.* **45** (4), 1807–1817. https://doi.org/10.1016/j.watres.2010.11.034.

Vreeburg, J. H. G. 2007 *Discolouration in Drinking Water Systems: A Particular Approach*. PhD thesis, Delft University of Technology, Delft, Netherland.

Vreeburg, J. H. G. & Boxall, J. B. 2007 Discolouration in potable water distribution systems: a review. *Water Res.* **41** (3), 519–529. https://doi.org/10.1016/j.watres.2006.09.028.

Zhou, X., Kosaka, K., Nakanishi, T., Welfringer, T. & Itoh, S. 2020 Manganese accumulation on pipe surface in chlorinated drinking water distribution system: contributions of physical and chemical pathways. *Water Res.* **184**, 116201. https://doi.org/10.1016/j.watres.2020.116201.

First received 28 May 2022; accepted in revised form 23 September 2022. Available online 28 September 2022